J. Plasma Phys. (2017), *vol.* 83, 705830106
doi:10.1017/S002237781700006X

Phase mixing importance for both Landau instability and damping

D. D. A. Santos[1],† **and Yves Elskens**[2],†

[1]Instituto de Física, Universidade de Brasília, CP: 04455, 70919-970 Brasília, DF, Brasil
[2]Aix-Marseille Université and CNRS, UMR 7345 PIIM, case 322, campus Saint-Jérôme, FR-13013 Marseille, France

(Received 28 October 2016; revised 18 January 2017; accepted 19 January 2017)

We discuss the self-consistent dynamics of plasmas by means of a Hamiltonian formalism for a system of N near-resonant electrons interacting with a single Langmuir wave. The connection with the Vlasov description is revisited through the numerical calculation of the van Kampen-like eigenfrequencies of the linearized dynamics for many degrees of freedom. Both the exponential-like growth as well as damping of the Langmuir wave are shown to emerge from a phase mixing effect among beam modes, revealing unexpected similarities between the stable and unstable regimes.

Key words: plasma dynamics, plasma instabilities, plasma waves

1. Introduction

Collisionless damping of electrostatic waves is one of the most fundamental phenomena in plasma physics and a starting point for the studies on the wave–particle interaction. From its first report by Landau (1946) until its experimental verification by Malmberg & Wharton (1964), this phenomenon was considered with some caution by the plasma community, in particular due to the mathematical aspects (specifically the use of complex integral and the large time limit in the Laplace transform) of its derivation and its paradoxical nature.

A very physical and intuitive approach was proposed by Dawson (1961), who explained this effect as resulting from a near-resonance mechanism of energy (and momentum) transfer between wave and particles. Dawson also pointed out a time threshold for a breakdown (due to trapping effects) of Landau's linear analysis. Later on, O'Neil (1965) extended the analysis for arbitrary times and found that the nonlinearities may lead the wave to a time-asymptotic behaviour with a constant non-zero amplitude. O'Neil's picture, introduced in the sixties, gave rise to what we call today 'nonlinear Landau damping' and induced a reconsideration of the phenomenon from experimental (Malmberg & Wharton 1967; Franklin, Hamberger & Smith 1972), numerical (Brodin 1997; Manfredi 1997) and theoretical (Mouhot & Villani 2010, 2011) viewpoints. In the last decades, the existence of a critical initial

† Email addresses for correspondence: daniel_dourado@yahoo.com.br, yves.elskens@univ-amu.fr

amplitude that distinguishes whether the asymptotic field Landau damps to zero or evolves to a steady non-zero value has been proved, by solving the Vlasov–Poisson system, by Brunetti, Califano & Pegoraro (2000) and Lancellotti & Dorning (2003) and from a statistical-physics-like viewpoint by Firpo & Elskens (2000, 2001).

Another prominent interpretation for linear Landau damping (beside Dawson's mechanical picture) explains it through the phase mixing of generalized (singular) eigenmodes of the corresponding linear dynamical system. This formulation, resting on a strictly linear theory and originally proposed by van Kampen (1955), shows that for a given perturbation with wavenumber k there is a continuous spectrum of real frequencies allowed for the plasma oscillations. In this context, Landau damping emerges from a special superposition of stationary (distribution-like) solutions that now go under the name of van Kampen modes. Though such superpositions account for the exponential decay of initial perturbations at Landau's rate, special initial data can also be constructed which cause a decay at slower rates (Belmont *et al.* 2011).

Nowadays, it is well known that other kinds of systems also admit normal modes analogous to the van Kampen modes for plasmas (see e.g. Pen 1994; Vekstein 1998; Vandervoort 2003). Indeed, similar phenomena are found in a wide variety of systems such as e.g. dusty plasmas (Bliokh, Sinitsin & Yaroshenko 1995), galaxies (Kandrup 1998), two-dimensional fluid flows (del Castillo-Negrete & Firpo 2002) and liquids containing gas bubbles (Smereka 2002). Despite its being an old problem, Landau damping remains intensely investigated experimentally (Doveil, Escande & Macor 2005) and theoretically (see e.g. Dougherty 1998; Ryutov 1999; del Castillo-Negrete 2002; Elskens 2005; Mouhot & Villani 2010, 2011; Bratanov *et al.* 2013; Bénisti 2016) with new aspects and viewpoints still being explored.

In contrast to the difficult reception of Landau damping by the physics community, the weak warm beam instability, captured by the same formula (with an opposite sign reflecting its physics), was immediately accepted. We show in this paper that its status is somewhat more subtle, and that this Landau instability has more to share with damping than might be thought initially. Indeed, the aim of this paper is to provide further theoretical and numerical insight into how both Landau effects emerge from the phase mixing among the van Kampen-like modes in the Hamiltonian approach.

The key element in plasmas is their being an N-body system*. Therefore, a microscopic description involving actual particles, rather than a continuum represented by a smooth distribution function in $(\boldsymbol{r}, \boldsymbol{v})$ space, is their physical fundamental model (Elskens & Escande 2003; Elskens, Escande & Doveil 2014). As deriving a kinetic model for singular interactions, with the Coulomb divergence at short range, remains a challenge (Chaffi, Casta & Brenig 2014; Kiessling 2014; Brenig, Chaffi & Rocha Filho 2016), understanding basic plasma phenomena from the N-body picture is important. Moreover, the N-body approach yields its own benefits, such as showing unexpected connections between Landau damping and Debye screening (Escande, Doveil & Elskens 2016).

The formalism adopted here is closely related to the fluid model used by Dawson (1960), where electrons are distributed into (almost) monokinetic beams, and the central issue consists in analysing normal modes that fully describe the evolution of the system. This approach is mathematically elementary, involving no partial differential equations or functional analysis and not even an analytic continuation or

*In the electrostatic description, where the interaction is described with the Poisson equation, the electric field is not even a dynamic degree of freedom. Though this is not the most complete picture of the plasma, it does account for several fundamental features of plasmas, including Landau damping and Debye shielding.

https://doi.org/10.1017/S002237781700006X Published online by Cambridge University Press

iε prescription enforcing a causality argument. Its concepts belong in basic classical mechanics.

In § 2, we revisit the Hamiltonian model for plasmas and waves (Escande, Zekri & Elskens 1996; Elskens & Escande 2003) and discuss connections with the van Kampen–Case approach (van Kampen 1955; Case 1959) when the continuous limit is taken. In § 3, we obtain the spectrum of the discrete analogue to the van Kampen frequencies by solving accurately the dispersion relation for systems composed of up to 2000 beams. We also investigate differences between the damping and growth regimes and the consistency between the discrete and the continuous systems by monitoring the evolution of the wave intensity.

Our main results show that not only the damping but also the Landau instability emerge as consequences of a phase mixing mechanism among the eigenmodes of the linear system. We highlight that while in the stable case the phase mixing to generate Landau damping involves all van Kampen-like eigenmodes, in the unstable case the pure Landau growth results from a destructive interference effect, leaving a single eigenmode having a dominant (exclusive, in the continuum limit) contribution to the wave amplitude. This behaviour, observed for dense spectrum systems, is described through (3.2) and its asymptotic form given in (3.3) and illustrated in figures 5 and 6.

The outcomes reported in this paper for systems with many degrees of freedom were made possible only by the development of a new technique to compute complex roots. This new root finding method is further detailed in appendix A.

2. Formalism of monokinetic beams

Our model system is composed of N charged resonant particles interacting with a single electrostatic Langmuir wave with natural frequency ω_0, in one space dimension (Onishchenko *et al.* 1970; O'Neil, Winfrey & Malmberg 1971). The evolution of this system is generated by the self-consistent Hamiltonian (Mynick & Kaufman 1978; Tennyson, Meiss & Morrison 1994; Escande *et al.* 1996; Elskens & Escande 2003; Escande 2010)

$$H_{sc} = \sum_{l=1}^{N} \frac{p_l^2}{2} + \omega_0 \frac{X^2+Y^2}{2} + \varepsilon k_w^{-1} \sum_{l=1}^{N} (Y \sin k_w x_l - X \cos k_w x_l), \tag{2.1}$$

where X and Y correspond to the Cartesian components of the complex wave amplitude $Z = X + \mathrm{i}Y$, also expressed as $Z = \sqrt{2I}\mathrm{e}^{-\mathrm{i}\theta}$ in terms of the phase θ and intensity I. We assume that particles have periodic boundary conditions in the interval of length L, and the wavenumber is $k_w = 2\pi j/L$ for some integer j. Parameter ε is the wave–particle coupling constant (which may be determined from further consideration of the underlying plasma).

The first and second terms in (2.1) represent the kinetic energy of the resonant particles (generating ballistic motion) and the energy of the free wave (related to the vibratory motion of the non-resonant bulk particles in the plasma), respectively. The latter (also responsible for the nonlinear nature of the dynamics) corresponds to the interaction energy between the wave and resonant particles.

The equations of motion are directly derived from the Hamiltonian (2.1),

$$\dot{x}_l = p_l, \quad 1 \leqslant l \leqslant N, \tag{2.2}$$

$$\dot{p}_l = \varepsilon \,\mathrm{Im}(Z\mathrm{e}^{\mathrm{i}k_w x_l}), \quad 1 \leqslant l \leqslant N, \tag{2.3}$$

https://doi.org/10.1017/S002237781700006X Published online by Cambridge University Press

$$\dot{Z} = -\mathrm{i}\omega_0 Z + \mathrm{i}\varepsilon k_w^{-1} \sum_{l'=1}^{N} \mathrm{e}^{-\mathrm{i}k_w x_{l'}}. \tag{2.4}$$

This dynamical system admits as equilibrium states the configurations where the electrostatic field has zero amplitude and the particles are distributed in monokinetic beams (as in Dawson's beams model), labelled $1 \leqslant s \leqslant b$, characterized by velocities v_s and number of particles N_s. Assuming

$$x_{ns}^{(0)}(t) = v_s t + nL/N_s + \phi_s \tag{2.5}$$

as the position of the nth particle of beam s with the number of particles per beam satisfying the condition $N_s > j$, the sum in (2.4) vanishes at any instant in time and, consequently, $(x_l(t) = x_{ns}^{(0)}(t), p_l(t) = v_s, Z(t) = 0)$ corresponds to an exact, equilibrium solution with vanishing wave. No similar solution exists with non-zero Z (Elskens 2001).

The dynamics preserves total energy H and total momentum $P = k_w I + \sum_l p_l$. The reversibility of Hamiltonian dynamics is expressed by the invariance of system (2.2)–(2.4) under the time-reversal map $(x', p', X', Y', t', H', k_w') = (x, -p, -X, Y, -t, H, -k_w)$. Here, the reversal of k_w accounts for the reversal of total momentum P under this map, as well as invariance of total energy H.

Considering the system slightly displaced from this equilibrium configuration, the evolution of the wave amplitude and the perturbations in particle orbits obey the linearized equations of motion

$$\delta\dot{x}_{ns} = \delta p_{ns}, \tag{2.6}$$

$$\delta\dot{p}_{ns} = -\varepsilon\, \mathrm{Im}(Z\mathrm{e}^{-\mathrm{i}k_w x_{ns}^{(0)}}), \tag{2.7}$$

$$\dot{Z} = -\mathrm{i}\omega_0 Z + \varepsilon \sum_{s=1}^{b} \sum_{n=1}^{N_s} \delta x_{ns} \mathrm{e}^{-\mathrm{i}k_w x_{ns}^{(0)}}, \tag{2.8}$$

where b is the number of beams ($\sum_{s=1}^{b} N_s = N$), $\delta x_{ns} = x_{ns} - x_{ns}^{(0)}$ and $\delta p_{ns} = p_{ns} - v_s$.

The perturbations in positions and momenta can be expressed in Fourier series with coefficients C and A (Escande *et al.* 1996),

$$\delta x_{ns}(t) = 2\,\mathrm{Im}(C_s(t)\mathrm{e}^{\mathrm{i}k_w x_{ns}^{(0)}(t)}) - \mathrm{i} \sum_{m \in \mu_s'} C_{ms}(t)\mathrm{e}^{\mathrm{i}k_m x_{ns}^{(0)}(t)}, \tag{2.9}$$

$$\delta p_{ns}(t) = 2\,\mathrm{Re}(A_s(t)\mathrm{e}^{\mathrm{i}k_w x_{ns}^{(0)}(t)}) + \sum_{m \in \mu_s'} A_{ms}(t)\mathrm{e}^{\mathrm{i}k_m x_{ns}^{(0)}(t)}, \tag{2.10}$$

where the set μ_s' is defined as

$$\mu_s' = \begin{cases} \{m \in \mathbb{Z} : |m| \leqslant (N_s - 1)/2 \text{ and } m \neq \pm j\}, & \text{if } N_s \text{ is odd,} \\ \{m \in \mathbb{Z} : 1 - N_s/2 \leqslant m \leqslant N_s/2 \text{ and } m \neq \pm j\}, & \text{if } N_s \text{ is even.} \end{cases} \tag{2.11}$$

The first terms in (2.9) and (2.10), which appear outside the sum, correspond to what we call the wave-like part of the solution. We omit the subscript j in the coefficients since they are the only components of the wave-like kind. The second terms, involving the sums over μ_s', corresponds to the ballistic parts whose evolutions are readily expressed in terms of the initial conditions,

$$C_{ms}(t) = (C_{ms}(0) + \mathrm{i}A_{ms}(0)t)\mathrm{e}^{-\mathrm{i}k_m v_s t} \tag{2.12}$$

https://doi.org/10.1017/S002237781700006X Published online by Cambridge University Press

$$A_{ms}(t) = A_{ms}(0)\mathrm{e}^{-\mathrm{i}k_m v_s t}, \tag{2.13}$$

because these terms do not couple with Z as $\sum_n \mathrm{e}^{-\mathrm{i}k_m x_{ns}^{(0)}} = 0$ for each m, s. On the contrary, due to their dependence on the wave amplitude Z, the wave-like components of the Fourier coefficients have a more intricate form that requires calculating the eigenvalues of the linearized system and expanding initial data in terms of the corresponding eigenvectors.

2.1. *Wave-like solution and dispersion relation*

The 'lattice' Fourier coefficients of the wave-like part satisfy the system of differential equations

$$\dot{C}_s = -\mathrm{i}k_w v_s C_s + \mathrm{i}A_s, \quad 1 \leqslant s \leqslant b, \tag{2.14}$$

$$\dot{A}_s = -\mathrm{i}k_w v_s A_s + \mathrm{i}\frac{\varepsilon}{2} Z, \quad 1 \leqslant s \leqslant b, \tag{2.15}$$

$$\dot{Z} = \mathrm{i}\omega_0 Z - \mathrm{i}\varepsilon \sum_{s=1}^{b} C_s N_s. \tag{2.16}$$

Assuming solutions of the form $\sim \mathrm{e}^{-\mathrm{i}\sigma t}$, the problem of solving the $2b+1$ equations of motion reduces to solving the algebraic linear system

$$\sigma \mathcal{C} = \boldsymbol{M} \cdot \mathcal{C}, \tag{2.17}$$

where $\mathcal{C} \in \mathbb{C}^{2b+1}$ denotes $\mathcal{C} = [c_1, \ldots, c_b, a_1, \ldots, a_b, z]^{\mathrm{T}}$, whose values of c_s and a_s represent, respectively, the time-independent part of the Fourier coefficients for the positions and momenta. The real matrix $\boldsymbol{M} \in \mathbb{R}^{(2b+1)\times(2b+1)}$ reads

$$\boldsymbol{M} = \begin{pmatrix} k_w v_1 & & 0 & -1 & & 0 & 0 \\ & \ddots & & & \ddots & & \vdots \\ 0 & & k_w v_b & 0 & & -1 & 0 \\ 0 & & 0 & k_w v_1 & & 0 & -\varepsilon/2 \\ & \ddots & & & \ddots & & \vdots \\ 0 & & 0 & 0 & & k_w v_b & -\varepsilon/2 \\ \varepsilon N_1 & \ldots & \varepsilon N_b & 0 & \ldots & 0 & \omega_0 \end{pmatrix}. \tag{2.18}$$

Denoting by $\mathcal{C}_r = [c_{r1}, \ldots, c_{rb}, a_{r1}, \ldots, a_{rb}, z_r]^{\mathrm{T}}$ the rth eigenvector of $\boldsymbol{M}$, its associated eigenvalue σ_r is obtained through the characteristic equation

$$\sigma_r = \omega_0 + \frac{\varepsilon^2}{2} \sum_{s=1}^{b} \frac{N_s}{(\sigma_r - k_w v_s)^2}. \tag{2.19}$$

For a given wavenumber k_w, (2.19) states the condition to be satisfied by the eigenfrequencies σ_r for the system (2.14)–(2.16) to admit non-trivial solutions. This equation is thus a dispersion relation for the eigenmodes of the linearized system. It can be transformed into a polynomial equation of degree $2b+1$ with real coefficients, and therefore admits generically $2b+1$ complex roots, with at least one of them purely real (see figure 1*b*).

https://doi.org/10.1017/S002237781700006X Published online by Cambridge University Press

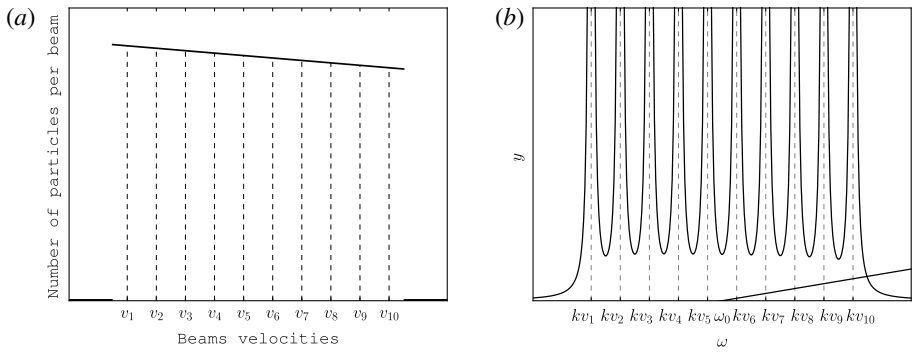

FIGURE 1. Illustration of a possible configuration for a system composed of one wave with natural frequency ω_0 and ten monokinetic beams. The beams velocities $v_s = v_1 + (s-1)\Delta p$ are set around the wave phase velocity ω_0/k. (*a*) Distribution of particles velocities with a constant slope, given according to $f(v_s) = f(v_1) + (s-1)\Delta p f'$ (yielding $N_s = N\Delta p f(v_s)$ as the number of particles) in $I_v = [v_1 - \Delta p/2,\, v_b + \Delta p/2]$ and set to zero outside this interval. (*b*) Graphical representation of the dispersion relation (2.19) through the line $y = \omega - \omega_0$ and the many branches curve $y = \chi(\omega) \equiv (\varepsilon^2/2)\sum_s (\omega - kv_s)^{-2} N_s$. The intercept point locates the single purely real solution to this equation.

The continuous limit corresponds to letting $N \to \infty$ while keeping $\varepsilon^2 N$ fixed. Particles are described with the distribution function (Firpo & Elskens 1998)

$$\mathcal{F}(x,p) = \lim_{N\to\infty} \frac{1}{N} \sum_l \delta(x - x_l)\delta(p - p_l) \tag{2.20}$$

and the wave is rescaled to

$$\mathcal{Z} = \varepsilon Z \tag{2.21}$$

so that the dynamics (2.2)–(2.3) generates the characteristics of the Vlasov equation

$$\partial_t \mathcal{F} + p\partial_x \mathcal{F} - \mathrm{Im}(\mathcal{Z} \mathrm{e}^{-\mathrm{i}k_w x})\partial_p \mathcal{F} = 0 \tag{2.22}$$

coupled with the wave evolution

$$\dot{\mathcal{Z}} = -\mathrm{i}\omega_0 \mathcal{Z} + \mathrm{i}k_w^{-1} \int_0^L \int_{-\infty}^{\infty} \mathrm{e}^{-\mathrm{i}k_w x} \mathcal{F}(x,p)\, \mathrm{d}p\, \mathrm{d}x. \tag{2.23}$$

The equilibrium reference state is $(\mathcal{Z} = 0,\ \mathcal{F}(x,\ v) = L^{-1} f(v))$, with the velocity distribution function such that $N_s = N \int_{v_s - \Delta p/2}^{v_s + \Delta p/2} f(p)\, \mathrm{d}p$: in the continuous limit, beam velocities are continuously distributed.

The dispersion relation in this limit follows from (2.19) by replacing the sum over the number of particles with an integral over the interval containing the beams velocities weighted by the normalized distribution $f(v_s)$. Formally, this leads to a singular integral equation if σ is real and $f(\sigma/k_w)$ does not vanish; with an $\mathrm{i}\epsilon$ prescription, Landau (1946) obtains a solution σ_L with imaginary part

$$\gamma_L = \frac{\pi \varepsilon^2 N}{2k_w^2} f'(\omega_0/k_w), \tag{2.24}$$

https://doi.org/10.1017/S002237781700006X Published online by Cambridge University Press

implying that the equilibrium is unstable for positive $f'(\omega_0/k_w)$ whereas perturbations are damped for negative $f'(\omega_0/k_w)$.

For equally spaced beams, $v_s - v_{s'} = (s-s')\Delta p$, analytical estimates (Dawson 1960; Escande *et al.* 1996; Elskens & Escande 2003) show that a pair of eigenvalues $\omega_r \pm \mathrm{i}\gamma_r$ is located near each beam (with $|v_s - \omega_r/k_w| < \Delta p/2$), with imaginary part

$$\gamma_r \simeq -\frac{1}{\tau_{rec}} \ln \left| \frac{\delta\sqrt{1+\theta_r^2}}{4\pi} \right| + \cdots, \tag{2.25}$$

where $\delta := f'(v_s)\Delta p/f(v_s)$ and $\theta_r = O(1)$. Their real part ω_r is near $(v_s + (\Delta p/4)\,\mathrm{sign}\,\delta)k_w$. The recurrence time

$$\tau_{rec} = \frac{2\pi}{k_j \Delta p} \tag{2.26}$$

characterizes the time scale on which the approximation of the many beams by a smooth distribution function loses its validity.

In the continuum limit, the imaginary parts $\pm\gamma_r$ of these eigenfrequencies as well as their spacing go to zero, so they approach a continuum spectrum of real eigenfrequencies which corresponds to the analogue of van Kampen modes found in the Vlasovian approach.

When the distribution function has a negative slope, there are $2b$ such van Kampen-like eigenvalues, and just one real eigenvalue beyond the fastest beam (see figure 1*b*). In contrast, for a positive $f'(\omega_0/k_w)$, besides these solutions condensing to the real axis in the limit, (2.19) is also satisfied by a particular pair of eigenvalues $\omega_L \pm \mathrm{i}\gamma_L$ whose imaginary part is given (in the limit $\Delta p \to 0$) by (2.24).

A first benefit of the discretized model with monokinetic beams is its avoiding singular integrals and prescriptions of proper integration contour inherent to the kinetic approach. It also stresses a deep difference between the damping and growth cases: despite their being encompassed by a single formula (2.24), they must involve different physics, because the instability is associated with a single eigenvalue solving (2.19), while in the damping case (2.19) admits no solution with negative imaginary part near γ_L.

This paradox reflects the reversibility of Hamiltonian dynamics: if damping resulted from a genuine eigenmode of the system, the dispersion relation would have a conjugate eigenvalue with positive real part, leading to an instability. This paradox of the Vlasov equation was solved by van Kampen (1955, 1957) and Case (1959).

A second indication that Landau damping does not result from the 'dominant eigenmode' in kinetic theory is that some initial data lead to a damping with smaller decay rate than Landau's: when present, they dominate over the Landau behaviour for long times (Belmont *et al.* 2011).

Actually, we shall see that both Landau damping and growth are related to a phase mixing effect among the van Kampen-like modes when the general solution of the linearized system is written in terms of its eigenfunctions.

2.2. *Normal modes expansion*

Denote by $\mathcal{C}_r$ and σ_r the rth eigenvector of $\boldsymbol{M}$ and its eigenvalue. Then, by the linearity of (2.17), the general solution $\mathcal{G}(t) = [C_1(t), \ldots, C_b(t), A_1(t), \ldots, A_b(t), Z(t)]^{\mathrm{T}}$ is a superposition of the eigensolutions $\mathcal{C}_r \mathrm{e}^{-\mathrm{i}\sigma_r t}$, i.e.

$$\mathcal{G}(t) = \sum_{r=1}^{2b+1} \xi_r \mathcal{C}_r \mathrm{e}^{-\mathrm{i}\sigma_r t}, \tag{2.27}$$

https://doi.org/10.1017/S002237781700006X Published online by Cambridge University Press

with components

$$C_s(t) = \frac{\varepsilon}{2} \sum_{r=1}^{2b+1} \frac{\xi_r}{(\sigma_r - k_w v_s)^2} \mathrm{e}^{-\mathrm{i}\sigma_r t}, \tag{2.28}$$

$$A_s(t) = \frac{\varepsilon}{2} \sum_{r=1}^{2b+1} \frac{\xi_r}{\sigma_r - k_w v_s} \mathrm{e}^{-\mathrm{i}\sigma_r t}, \tag{2.29}$$

$$Z(t) = \sum_{r=1}^{2b+1} \xi_r \mathrm{e}^{-\mathrm{i}\sigma_r t}. \tag{2.30}$$

The coefficients ξ_r of the linear combination are obtained from the initial condition and the left eigenvectors of matrix $\boldsymbol{M}$, $\sigma_r \mathcal{C}'_r = \boldsymbol{M}^{\mathrm{T}} \cdot \mathcal{C}'_r$, through the inner product

$$\xi_r = \mathcal{C}'^{\mathrm{T}}_r \cdot \mathcal{G}(0) = z'_r \left[Z(0) + \varepsilon \sum_{s=1}^{b} N_s \left(\frac{C_s(0)}{\sigma_r - k_w v_s} - \frac{A_s(0)}{(\sigma_r - k_w v_s)^2} \right) \right], \tag{2.31}$$

where the scaling factor z'_r, given by

$$z'_r = \left[1 + \varepsilon^2 \sum_{s=1}^{b} \frac{N_s}{(\sigma_r - k_w v_s)^3} \right]^{-1}, \tag{2.32}$$

is chosen so that the normalization condition $\mathcal{C}'^{\mathrm{T}}_{r'} \cdot \mathcal{C}_r = \delta_{r',r}$ is satisfied.

In the linear regime, the system of beams interacting with a single Langmuir wave is therefore analytically solvable in terms of a normal modes expansion of the linearized equations of motion. Within the present approach, specifically through (2.9)–(2.13) and (2.27)–(2.32), note that once the full spectrum of eigenfrequencies $\{\sigma_r\}$ and the initial condition of the dynamics (the coefficients ξ_r) are known, the evolution of the wave amplitude and the perturbations on the particles orbits are determined.

In particular, the scaling factor z'_r coincides with the weight of eigenvector $\mathcal{C}_r$ in the decomposition of a 'quiet start' initial condition ($\delta x_{ns}(0) = 0$, $\delta p_{ns}(0) = 0$, *viz.* $C_s(0) = 0, A_s(0) = 0$).

3. Numerical results and discussion

In this section, we discuss the spectrum of the van Kampen-like eigenfrequencies obtained by solving numerically (2.19) for many-beam systems and stress some microscopic aspect of the dynamics. As we shall see, both wave damping and growth arise as consequence of an interference among the $2b + 1$ eigenmodes. However, in respect to this interference (or phase mixing) effect, these two cases exhibit a remarkable distinctive behaviour as the number of beams becomes large.

The monokinetic beams approach presented in § 2 breaks down after times of the order of the bouncing time $\omega_b^{-1} = (\varepsilon |Z| k_w)^{-1/2}$, where the particle orbit may no longer be considered approximately ballistic. To ensure that trapping effects play a negligible role and the structure of beams is preserved, all the following results were obtained in the weak amplitude regime (easily implemented in taking $\varepsilon \ll 1$, $N \sim \varepsilon^{-2} \to \infty$). To simplify our numerical calculations, we take $\omega_0 = 0.0$

https://doi.org/10.1017/S002237781700006X Published online by Cambridge University Press

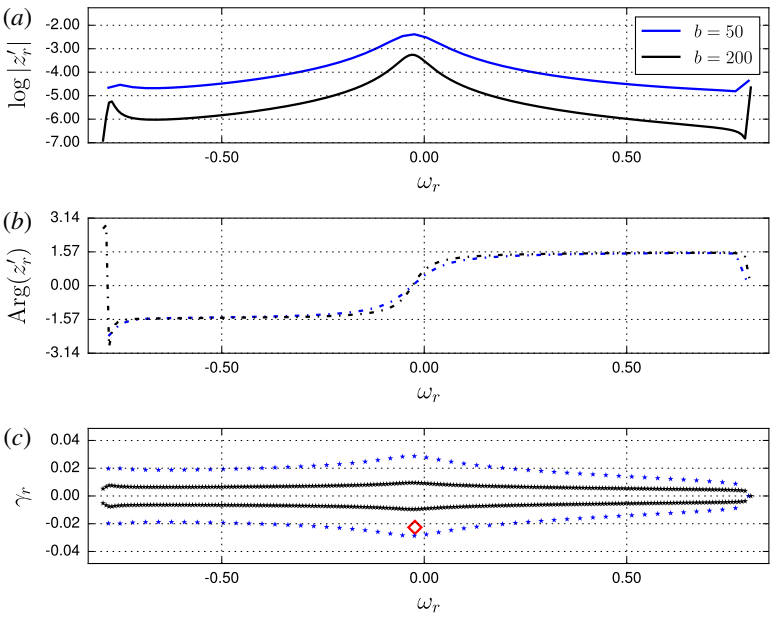

FIGURE 2. Damping case: discrete analogue of van Kampen eigenfrequencies in the complex σ – plane (c), the phase (b) and the modulus (a) of the scaling factor. The curves in the two upper panels are guides to the eye. The red losangle locates the Landau value σ_L (which corresponds to no eigenmode in the finite-N model). The results were obtained for systems composed of 50 and 200 beams with parameters set to $I_v = 1.6$, $\omega_0 = 0.0$, $k_w = 1.0$, $\varepsilon N f' = -4.8$ and $\gamma_L = -2.26 \times 10^{-2}$.

which, from the physical viewpoint, amounts to performing a Galileo transformation to a reference frame moving with the wave (nominal) phase velocity. We set the equilibrium state with particle velocities equally spaced ($v_s = v_1 + (s-1)\Delta p$) inside an interval of length I_v centred at the origin and the distribution function $f(v_s) = f(v_1) + (s-1)f'\Delta p$, where f' is constant and $\Delta p = I_v/b$ is the velocity interval between two adjacent beams. The data $f(v_1) = 1/I_v - (b-1)\Delta p f'/2$ ensure that the distribution of velocities is normalized to unity. Thus, the number of particles[†] in beam s is given by $N_s = N\Delta p f(v_s)$.

In the weak-coupling regime and for many-beam systems, the spectrum of eigenfrequencies is very close to the real axis, and therefore the numerical solutions of (2.19) must be computed with high accuracy. To obtain the spectrum of eigenfrequencies for such systems with an accuracy down to 10^{-7} ($|\sigma_r^{approx} - \sigma_r| \leqslant 10^{-7}$), we developed a root-finding scheme based on Cauchy's residue theorem with triangular contours that enabled us to implement a bisection method in the complex σ-plane. In this paper, we shall not dwell on the technical details of the method; its key ideas are discussed in appendix A.

3.1. *Spectra and scaling factors*

In the lowest graph in figure 2, we plot the spectrum of van Kampen-like eigenfrequencies for the damping case ($f' < 0$) for systems composed of 50 and 200

[†]Formally, one may wish N_s to be integer. However, the linear dynamics (2.14)–(2.16) for Fourier coefficients no longer refers to individual particles, and any real positive values for N_s/N, N and εN are mathematically admissible. Rational or integer values are not remarkable in this context.

https://doi.org/10.1017/S002237781700006X Published online by Cambridge University Press

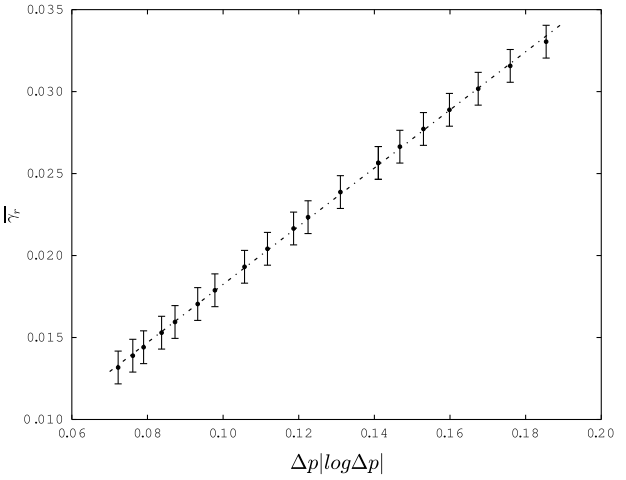

FIGURE 3. Damping case: behaviour of the average distance to real axis $\bar{\gamma}_r \equiv b^{-1} \sum_{r,\gamma_r>0} \gamma_r$ as a function of the beam spacing. The linear regression $y = (0.177 \pm 0.001)x \pm 0.001$ shows that γ_r goes to zero like $x \equiv \Delta p\,|\log \Delta p|$ as computed by Dawson (1960). The error bars represent the tolerance 10^{-3} used in the root-finding routine.

beams. The upper two plots display the logarithm of the modulus of the scaling factor z'_r and its phase $\mathrm{Arg}\, z'_r$, obtained from the spectra and (2.32). These curves correspond only to the eigenmodes with $\gamma_r \geqslant 0$: thanks to the time reversibility of Hamiltonian dynamics implying real coefficients in the algebraic equation (2.32), the stable eigenmodes differ only by the opposite sign of their phase. Regardless of the number of beams, the phase velocities ω_r/k_w of the damped and growing eigenmodes are confined to the interval $[-0.8, 0.8]$ that contains the resonant particles. The more beams we consider, denser the spectrum becomes and it approaches as a whole the real axis. The dependence of the mean value of the imaginary part $\bar{\gamma}_r = b^{-1} \sum_{r,\gamma_r>0} \gamma_r$ (which amounts to the ℓ^1 norm of the sequence of these imaginary parts) on the beam spacing is illustrated in figure 3, indicating how, in the continuous limit ($\Delta p \to 0$), these eigenfrequencies accumulate toward the real axis forming what corresponds to the continuous spectrum of van Kampen frequencies derived from a Vlasovian description. The spacing between the real parts of successive eigenfrequencies also goes to zero like Δp because there is always a real ω_r/k_w between two successive beam velocities, so that the condensation of eigenvalues onto the real axis tends to a cut along the interval $[\inf(v_s), \sup(v_s)]$: this cut is the locus of van Kampen's singular spectrum. This behaviour $\gamma_r \sim \Delta p\,|\ln \Delta p|$, (2.25) was computed by Dawson (1960).

Landau's value $\sigma_L = \omega_L + \mathrm{i}\gamma_L$, represented by the red diamond point in figure 2, is obtained after taking the continuous limit of (2.19). The interaction between the wave and resonant particles is responsible for the small deviation $|\omega_L - \omega_0| = 2.30 \times 10^{-2}$ from the free wave frequency, which can also be estimated analytically (Elskens & Escande 2003).

We also observe, in the vicinity of ω_L, a striking behaviour for the modulus and for the phase of the scaling factor. The top plot evidences a peak slightly shifted from the origin, and the centre plot shows a change in the phase's sign. These two behaviours together indicate that the modes with greater contribution to the initial data $(\delta x_{ns}(0), \delta p_{ns}(0), Z(0))$ are those with a frequency close to the Landau value, in

https://doi.org/10.1017/S002237781700006X Published online by Cambridge University Press

agreement with the estimate (Elskens & Escande 2003)

$$z'_r \simeq -\frac{1}{2\pi}\frac{k_w \Delta p}{\gamma_L \pm \mathrm{i}(\omega_r - \omega_L)} \tag{3.1}$$

from (2.32). The plus-or-minus sign in this equation take care of the two r eigenmodes with same phase velocity.

For the growth case ($f' > 0$), the spectrum and the scaling factor shown in figure 4 exhibit two distinctive features (compared to the damping regime) for systems with many beams. The first one is the presence of two specific eigenfrequencies, complex conjugate to each other, that do not approach the real axis as the number of beams increase. We denote the eigenfrequency close to the Landau frequency by σ_{bL} (Landau-like eigenmode, with subscript b recalling the finite number of beams) and its complex conjugate by σ_{bL^*} (anti-Landau eigenmode), both highlighted in the figure. The second striking difference is the spike (note the log scale) in the curve for the modulus of the scaling factor. It shows, along with $\mathrm{Arg}(z'_{bL}) \approx 0$, that the Landau and the anti-Landau eigenmodes have a dominant contribution to the initial data.

3.2. *Quiet start evolution*

In order to monitor the contributions of the bL and bL^* eigenmodes to the wave amplitude, we consider a single realization of the system where the wave is launched with initial amplitude $Z(0) = 1$ and particles start from the equilibrium configuration of monokinetic arrays. For this specific quiet start realization, the evolution of the wave amplitude is given according to (2.30) by

$$Z(t) = z'_{bL}\mathrm{e}^{-\mathrm{i}\sigma_{bL}t} + z'_{bL^*}\mathrm{e}^{-\mathrm{i}\sigma_{bL^*}t} + \sum_{\substack{r=1 \\ r\neq bL, bL^*}}^{2b+1} z'_r \mathrm{e}^{-\mathrm{i}\sigma_r t}, \tag{3.2}$$

recalling that the scaling factor corresponds to a weight factor indicating how much each eigenmode contributes to construct the initial amplitude.

Due to the fact that for many-beam systems $z'_{bL} \approx 1$ and $\sigma_{bL} \approx \sigma_L$, as seen from the black graphs in figure 4, one would expect the Landau-like (bL) eigenmode to provide, by itself, the correct growth of the wave. However, the contribution of the other $2b$ eigenmodes still have to be taken into account. Thanks to a destructive interference, these $2b$ eigenmodes superposed contribute only with a small oscillatory part that does not compromise the exponential growth $\sim \mathrm{e}^{\gamma_L t}$ of the wave. Figure 5 illustrate this destructive interference by monitoring the evolution of the Cartesian components of each term of (3.2) for a system of 2000 beams. This graph exhibits a clear symmetry between the red and green curves, showing that the $O(1)$ contribution of the anti-Landau eigenmode is cancelled out by the superposition of the (dense, individually small) van Kampen-like eigenmodes. The dashed curves that appear as an envelope in figure 5 are given by $\pm\mathrm{e}^{-\gamma_L t}$ and indicate that, in the same way as for the anti-Landau eigenmode, the superposition of the van Kampen-like eigenmodes also damps with the anti-Landau rate.

Analytically, indeed, the asymptotic form (3.1) for the scaling factor implies that the third term in (3.2) behaves like the Fourier transform of a Lorentz function, namely as $-Z(0)\mathrm{e}^{-\gamma_L|t|}$. Therefore, (3.2) reduces to

$$Z(t) \simeq Z(0)\mathrm{e}^{\gamma_L t} + Z(0)\mathrm{e}^{-\gamma_L t} - Z(0)\mathrm{e}^{-\gamma_L|t|} \tag{3.3}$$

which reduces to $Z(0)\mathrm{e}^{\gamma_L|t|}$ for both positive and negative t.

https://doi.org/10.1017/S002237781700006X Published online by Cambridge University Press

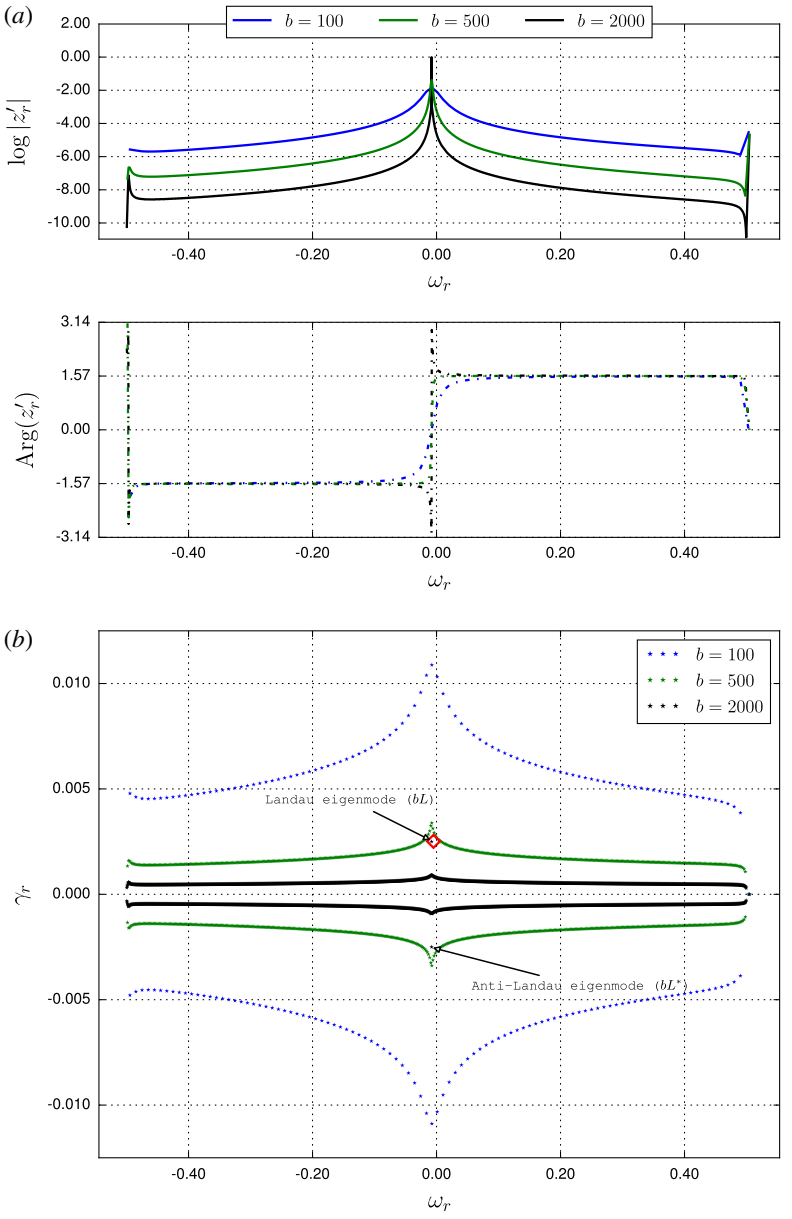

FIGURE 4. Growth case: (*a*) modulus and phase of the scaling factor (the lines are guides to the eye) and (*b*) spectrum of the van Kampen-like eigenfrequencies in the complex σ plane for systems composed of 100, 500 and 2000 beams. The red losangle locates the Landau mode, which is slightly shifted from the origin by $\omega_L = -4.87 \times 10^{-3}$. The parameters were set to $I_v = 1.0$, $\omega_0 = 0.0$, $k_w = 1.0$, $\varepsilon N f' = 16.0$ and $\gamma_L = 2.51 \times 10^{-3}$.

This form rescues the time reversibility in the solution to the initial value problem. If the response to the initial perturbation were described with only the Landau-like eigenmode, it would lead to a decreasing $|Z(t)|$ for $t \to -\infty$. Yet time-reversal symmetry (unbroken by the quiet start initial condition) requires the wave to increase

https://doi.org/10.1017/S002237781700006X Published online by Cambridge University Press

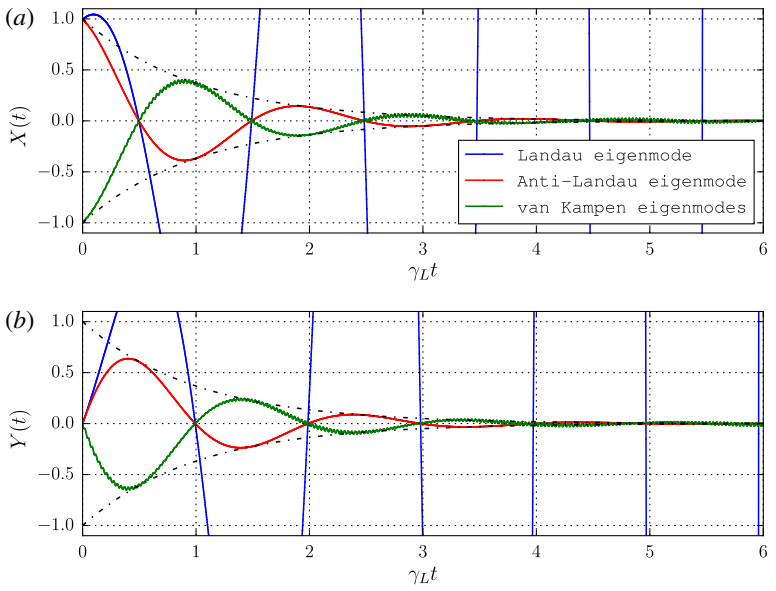

FIGURE 5. Growth case: evolution of real (a) and imaginary (b) parts of the Landau (bL), anti-Landau (bL^*) and van Kampen-like components in the wave complex amplitude $Z = X + \mathrm{i}Y$ for a system of 2000 beams in the unstable case. The symmetry between the red and green curves shows the compensation between the anti-Landau eigenmode and the van Kampen spectrum. The Landau (blue) line is growing exponentially, exceeding largely the range of our ordinate axis.

as $t \to -\infty$ just as it does for $t \to \infty$. Therefore, the system evolution for all times must involve both the Landau-like and anti-Landau modes, the sum of which reads $2Z(0)\cosh\gamma_L t$. But this sum does not start exactly exponentially at $t = 0$, so that the van Kampen-like eigenmodes are needed to cancel the anti-Landau mode for $t > 0$, and to cancel the Landau-like mode for $t < 0$.

This peculiarity of the growth regime can be seen numerically only when considering a larger number of beams. The necessity of working with such many-beam systems motivated us to developed the Cauchy root-finding scheme once that traditional computer algebra systems failed in providing the full spectrum.

Note that the damping case is analytically simpler: it involves only van Kampen-like eigenmodes, for which the scaling factors given by (3.1) again yield the Fourier transform of a Lorentz function. However, γ_L is now negative, so that $z_r' > 0$ for $\omega_r \approx \omega_L$ and (3.2) reduces to the well known

$$Z(t) \simeq Z(0)\mathrm{e}^{\gamma_L|t|}. \tag{3.4}$$

Figure 6 show the evolution of the wave intensity $I = Z^*Z/2$, obtained through the superposition of the van Kampen-like eigenmodes for systems composed of 30, 50 and 200 beams. We observe that the Langmuir wave damps (or grows) initially with the expected Landau prediction $\log I_L(t) = \log I(0) \pm 2|\gamma_L|t$, represented by the dashed black lines. For the unstable case, even for a small number of beams, where $\max\{\gamma_r\} > \gamma_L$ and the bL and bL^* modes are not prominent, the discrete and continuous systems agree.

https://doi.org/10.1017/S002237781700006X Published online by Cambridge University Press

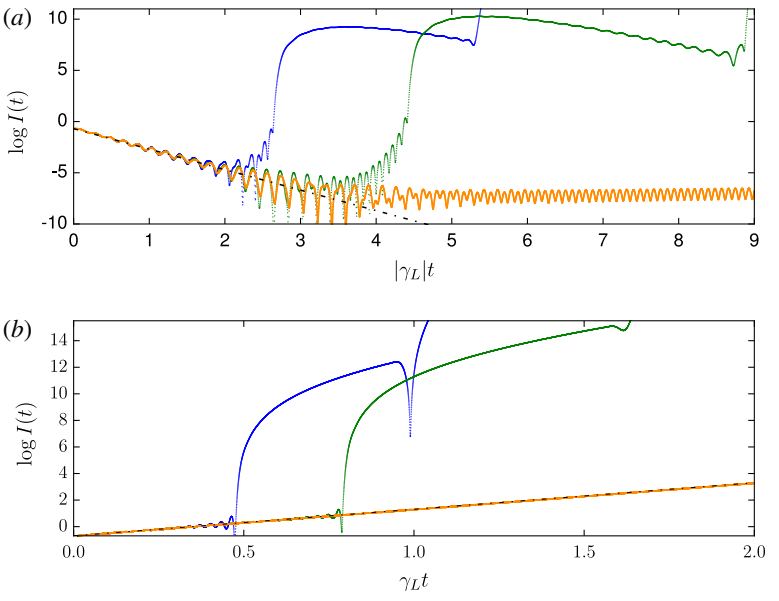

FIGURE 6. Evolution of the wave intensity for systems composed of 30 (red), 50 (blue) and 200 (orange) beams for the stable (*a*) and the unstable (*b*) cases with the dashed lines corresponding to the Landau prediction. The same parameters that generated the spectra in figures 2 and 4 were used here. As initial condition we consider $Z(0) = 1.0$ and unperturbed trajectories $\delta x_{ns}(0) = \delta p_{ns}(0) = 0$ with particles starting in the configuration of equally spaced monokinetic beams.

The divergences observed in the graphs occur for times close to the recurrence time $\tau_{rec} \sim 2\pi/\Delta\omega_r \sim 2\pi/(k_w \Delta p)$ where the lack of an effective phase mixing of the van Kampen-like eigenmodes along with the large values of the modulus of the complex amplitude $z'_r e^{\gamma_r t}$ of the unstable eigenmodes make the wave intensity depart from the Landau line. After this characteristic time, the approximation of a discrete system composed of monokinetic beams by a continuous one is no longer valid (Firpo & Elskens 1998). It is worth noting that the departure of the orange curve from the Landau line in the top part of figure 6 is not related to the breakdown of the phase mixing but to the small values of $I_L(t)$ compared to the amplitude of the oscillations.

4. Summary and perspectives

Our results in this paper provide an accurate numerical support for studying the phase mixing mechanism in Hamiltonian models. Success in investigating this process for many-beams systems rests on the development of a new root finding scheme based on the Cauchy's integral theorem enabling one to compute all the roots of the dispersion relation (2.19).

Analysing the spectrum of eigenfrequencies of the van Kampen-like modes and the evolution of the Cartesian components of the wave amplitude highlights a remarkable aspect in which the stable and unstable regimes differ. In the stable case, the normal modes simply contribute collectively in providing the Landau damping; however, in the unstable case, the pure exponential growth of the wave amplitude is the result of a destructive interference effect (between its dual exponentially decaying mode,

https://doi.org/10.1017/S002237781700006X Published online by Cambridge University Press

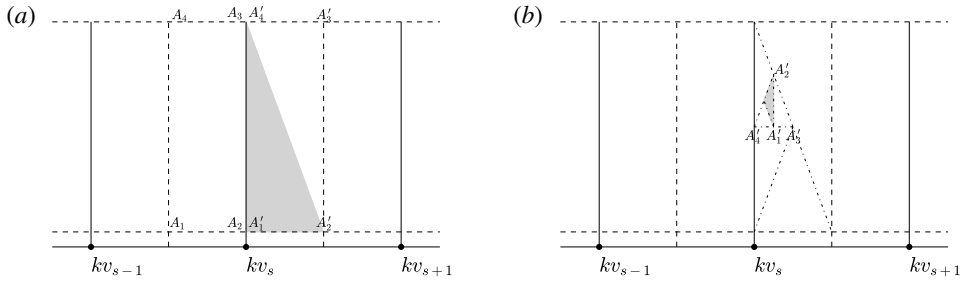

FIGURE 7. Illustration of the bisection-like method in the complex σ-plane by supposing that the root is located to the right side of the line corresponding to the sth beam. The shaded triangles highlight the regions for which the contour integral is non-zero and that, consequently, contain a root inside.

with same initial amplitude, and a flurry of van Kampen modes with small individual amplitudes) that enables a single eigenmode to provide a dominant contribution on the dynamics from the very beginning. We conclude the paper pointing out the consistence between the discrete and the continuous systems (Firpo & Elskens 1998), and verifying that the superposition of the van Kampen-like eigenmodes indeed provides the expected exponential Landau damping/growth rate for the wave intensity.

The quiet start as well as the equally spaced beams setting were chosen in order to simplify the calculations. However, one expects similar results for other discretizations and initial conditions of the system in the many beams regime.

Acknowledgements

The first author thanks Coordenação de Aperfeiçoamento de Pessoal de Nível Superior (CAPES) for financing his stay at Aix-Marseille Université under the Programa de Doutorado Sanduíche no Exterior (PDSE), process no. 99999.004512/2014-06. Valuable discussions with B. V. Ribeiro and comments from D. F. Escande, M. A. Amato, F. Doveil and D. F. G. Minenna are gratefully acknowledged. The authors also acknowledge the reviewers for their useful comments.

Appendix A. Bisection-like root finding method in the complex plane

The Cauchy integral theorem states that if F is an analytic function on a simply connected domain $\mathcal{D}$ bounded by a simple closed contour $\partial\mathcal{D}$, then $\oint_{\partial D} F(z)\,\mathrm{d}z = 0$, and if F has a finite number of simple poles z_j in $\mathcal{D}$ with residues R_j, then $\oint_{\partial D} F(z)\,\mathrm{d}z = 2\pi\mathrm{i}\sum_j R_j$. In this appendix, we expose a direct scheme based on this elementary tool of complex analysis with the aim of computing numerically the full set of van Kampen-like eigenfrequencies.

With $\chi(\sigma)$ being the right-hand side of (2.19), the method consists in obtaining the root of $\sigma - \chi(\sigma)$, inside a given region, by searching for the pole of $(\sigma - \chi(\sigma))^{-1}$. To find a root in the vicinity of the velocity of the sth beam, we define two rectangles: the left one with vertices A_1 to A_4 and the right one with vertices A_1' to A_4', both illustrated in figure 7(*a*). Firstly, we estimate the Cauchy integral along these rectangular contours in order to identify to which side from the sth beam the root is located. If one of these rectangles yields

$$\left|\oint_{\partial\mathcal{D}} (\sigma - \chi(\sigma))^{-1}\,\mathrm{d}\sigma\right| \leqslant C_{crit}, \tag{A 1}$$

https://doi.org/10.1017/S002237781700006X Published online by Cambridge University Press

with C_{crit} representing the Cauchy criterion to assume the integral numerically zero, it is discarded as a possible region containing the root.

After identifying the presence of a root inside a rectangle, the next step consists in implementing the bisection-like method which is based on successive divisions of the region of search. In figure 7, we illustrate this procedure with the shaded triangles in figures 7(*a*) and 7(*b*) showing, respectively, the configuration at the beginning and after 6 iterations of the method. Iterations are stopped when the largest side of the shaded triangle is smaller than the tolerance of the method (which is an input data). Following so, the approximate root of $\sigma - \chi(\sigma)$ is given by the geometrical centre of the triangle.

ALGORITHM 1. BISECTION-LIKE ROOT FINDING METHOD

```
Gside ← Larger_side (A'1, A'2, A'4)
root ← NULL
if ¬exist_pole_inside (A'1, A'2, A'4) then
  if ¬exist_pole_inside (A'3, A'2, A'4) then
    return root
  else
    A'1 ← A'3
    A'3 ← A'4
    A'4 ← A'2
    A'2 ← A'3
  end if
end if

while Gside ⩾ error do
  if exist_pole_inside (A'1, (A'2 + A'4)/2, A'4) then
    A'3 ← A'2
    A'2 ← A'4
    A'4 ← A'1
    A'1 ← (A'2 + A'3)/2
  else
    A'3 ← A'4
    A'4 ← A'2
    A'2 ← A'1
    A'1 ← (A'3 + A'4)/2
  end if
  Gside ← Larger_side (A'1, A'2, A'4)
end while
root ← (A'1 + A'2 + A'4)/3
return root
end
```

The bisection-like method is displayed through the pseudo-code in Algorithm 1, where we called the function 'Larger_side (A,B,C)', that yields the length of the largest side of triangle ABC, and the function 'exist_pole_inside (A,B,C)' whose Boolean output informs, by means of the Cauchy criterion (A 1), whether there is a pole of $(\sigma - \chi(\sigma))^{-1}$ inside the triangle ABC. The code generating the results in this paper was implemented in C language with the 'complex.h' library.

https://doi.org/10.1017/S002237781700006X Published online by Cambridge University Press

Although the method was built specifically to tackle the problem of monokinetic beams presented in this paper, it can *a priori* be used in an efficient way to find the complex roots of any function $F(\sigma)$ which is well behaved in the integration domains and such that the poles of $F^{-1}(\sigma)$ have non-vanishing residues.

REFERENCES

BELMONT, G., CHUST, TH., MOTTEZ, F. & HESS, S. 2011 Landau and non-Landau linear damping: physics of the dissipation. *Transp. Theory Stat. Phys.* **40**, 419–424.

BÉNISTI, D. 2016 Envelope equation for the linear and nonlinear propagation of an electron plasma wave, including the effects of Landau damping, trapping, plasma inhomogeneity, and the change in the state of wave. *Phys. Plasmas* **23**, 102105.

BLIOKH, P., SINITSIN, V. & YAROSHENKO, V. 1995 *Dusty and Self-gravitational Plasmas in Space*. Kluwer.

BRATANOV, V., JENKO, F., HATCH, D. & BRUNNER, S. 2013 Aspects of linear Landau damping in discretized systems. *Phys. Plasmas* **20**, 022108.

BRENIG, L., CHAFFI, Y. & ROCHA FILHO, T. M. 2016 Long velocity tails in plasmas and gravitational systems. arXiv:1605.05981.

BRODIN, G. 1997 Nonlinear Landau damping. *Phys. Rev. Lett.* **78**, 1263–1266.

BRUNETTI, M., CALIFANO, F. & PEGORARO, F. 2000 Asymptotic evolution of nonlinear Landau damping. *Phys. Rev.* E **62**, 4109–4114.

CASE, K. M. 1959 Plasma oscillations. *Ann. Phys.* **7**, 349–364.

DEL CASTILLO-NEGRETE, D. 2002 Dynamics and self-consistent chaos in a mean field Hamiltonian model. In *Dynamics and Thermodynamics of Systems with Long-range Interactions* (ed. Th. Dauxois, S. Ruffo, E. Arimondo & M. Wilkens), Lecture Notes in Physics, vol. 602, pp. 407–436. Springer.

DEL CASTILLO-NEGRETE, D. & FIRPO, M.-CH. 2002 Coherent structures and self-consistent transport in a mean field Hamiltonian model. *Chaos* **12**, 496–507.

CHAFFI, Y., CASTA, R. & BRENIG, L. 2014 Effect of the fluctuations around mean field for *N*-body systems with long range interactions. arXiv:1401.4746.

DAWSON, J. M. 1960 Plasma oscillations of a large number of electron beams. *Phys. Rev.* **118**, 381–389.

DAWSON, J. M. 1961 On Landau damping. *Phys. Fluids* **4**, 869–874.

DOUGHERTY, J. P. 1998 Van Kampen modes revisited. *J. Plasma Phys.* **59**, 629–637.

DOVEIL, F., ESCANDE, D. F. & MACOR, A. 2005 Experimental observation of nonlinear synchronization due to a single wave. *Phys. Rev. Lett.* **94**, 085003.

ELSKENS, Y. 2001 Finite-*N* dynamics admit no traveling-wave solutions for the Hamiltonian XY model and single-wave collisionless plasma model. *ESAIM: Proc.* **10**, 211–215.

ELSKENS, Y. 2005 Irreversible behaviours in Vlasov equation and many-body Hamiltonian dynamics: Landau damping, chaos and granularity in the kinetic limit. In *Topics in Kinetic Theory* (ed. Th. Passot, C. Sulem & P.-L. Sulem), Fields Institute Communications Series, vol. 46, pp. 89–108. American Mathematical Society.

ELSKENS, Y. & ESCANDE, D. 2003 *Microscopic Dynamics of Plasmas and Chaos*. IOP.

ELSKENS, Y., ESCANDE, D. F. & DOVEIL, F. 2014 Vlasov equation and *N*-body dynamics: how central is particle dynamics to our understanding of plasmas? *Eur. Phys. J.* D **68**, 218.

ESCANDE, D. F. 2010 Wave-particle interactions in plasmas: a qualitative approach. In *Long-range Interacting Systems* (ed. Th. Dauxois, S. Ruffo & L. F. Cugliandolo), Les Houches Summer School, vol. XC, pp. 469–506. Oxford University Press.

ESCANDE, D. F., DOVEIL, F. & ELSKENS, Y. 2016 *N*-body description of Debye shielding and Landau damping. *Plasma Phys. Control. Fusion* **58**, 014040.

ESCANDE, D. F., ZEKRI, S. & ELSKENS, Y. 1996 Intuitive and rigorous derivation of spontaneous emission and Landau damping of Langmuir waves through classical mechanics. *Phys. Plasmas* **20**, 3534–3539.

https://doi.org/10.1017/S002237781700006X Published online by Cambridge University Press

FIRPO, M.-CH. & ELSKENS, Y. 1998 Kinetic limit of N-body description of wave–particle self-consistent interaction. *J. Stat. Phys.* **93**, 193–209.

FIRPO, M.-CH. & ELSKENS, Y. 2000 Phase transition in the collisionless damping regime for wave–particle interaction. *Phys. Rev. Lett.* **84**, 3318–3321.

FIRPO, M.-CH. & ELSKENS, Y. 2001 O'Neil's threshold for nonlinear Landau damping and phase transition in the wave–particle system. *ESAIM: Proc.* **10**, 217–222.

FRANKLIN, R. N., HAMBERGER, S. M. & SMITH, G. J. 1972 Damping of finite-amplitude electron plasma waves in a collisionless plasma. *Phys. Rev. Lett.* **29**, 915–917.

VAN KAMPEN, N. G. 1955 On the theory of stationary waves in plasmas. *Physica* **XXI**, 949–963.

VAN KAMPEN, N. G. 1957 The dispersion equation for plasma waves. *Physica* **XXIII**, 641–650.

KANDRUP, H. E. 1998 Violent relaxation, phase mixing, and gravitational Landau damping. *Astrophys. J.* **500**, 120–128.

KIESSLING, M. K.-H. 2014 The microscopic foundation of Vlasov theory for jellium-like Newtonian N-body systems. *J. Stat. Phys.* **155**, 1299–1328.

LANCELLOTTI, C. & DORNING, J. J. 2003 Time-asymptotic wave propagation in collisionless plasmas. *Phys. Rev.* E **68**, 026406.

LANDAU, L. D. 1946 On the vibrations of the electronic plasma. *J. Phys. USSR* **10**, 25–34.

MALMBERG, J. H. & WHARTON, C. B. 1964 Collisionless damping of electrostatic plasma waves. *Phys. Rev. Lett.* **13**, 184–186.

MALMBERG, J. M. & WHARTON, C. B. 1967 Collisionless damping of large-amplitude plasma waves. *Phys. Rev. Lett.* **19**, 775–777.

MANFREDI, G. 1997 Long-time behavior of nonlinear Landau damping. *Phys. Rev. Lett.* **79**, 2815–2818.

MOUHOT, C. & VILLANI, C. 2010 Landau damping. *J. Math. Phys.* **51**, 015204.

MOUHOT, C. & VILLANI, C. 2011 On Landau damping. *Acta Mathematica* **207**, 29–201; corr. fig. 391.

MYNICK, H. E. & KAUFMAN, A. N. 1978 Soluble theory of nonlinear beam–plasma interaction. *Phys. Fluids* **21**, 653–663.

O'NEIL, T. 1965 Collisionless damping of nonlinear plasma oscillations. *Phys. Fluids* **8**, 2255–2262.

O'NEIL, T. M., WINFREY, J. H. & MALMBERG, J. H. 1971 Nonlinear interaction of a small cold beam and a plasma. *Phys. Fluids* **14**, 1204–1212.

ONISHCHENKO, I. N., LINETSKIĬ, A. R., MATSIBORKO, N. G., SHAPIRO, V. D. & SHEVCHENKO, V. I. 1970 Contribution to the nonlinear theory of excitation of a monochromatic plasma wave by an electron beam. *Zh. Eksp. Teor. Fiz. Pis. Red.* **12**, 407–411; transl. *JETP Lett.* **12**, 281–285.

PEN, U.-L. 1994 Modes of elliptical galaxies. *Astrophys. J.* **431**, 104–108.

RYUTOV, D. D. 1999 Landau damping: half a century with the great discovery. *Plasma Phys. Control. Fusion* **41** (Suppl. 3A), A1–A12; Proc. EPS Conf. Control. Fusion Plasma Phys. and Intl Cong. Plasma Phys. Prague 1998.

SMEREKA, P. 2002 A Vlasov equation for pressure wave propagation in bubbly fluids. *J. Fluid Mech.* **454**, 287–325.

TENNYSON, J. L., MEISS, J. D. & MORRISON, P. J. 1994 Self-consistent chaos in the beam–plasma instability. *Physica* D **71**, 1–17.

VANDERVOORT, P. O. 2003 On stationary oscillations of galaxies. *Mon. Not. R. Astron. Soc.* **339**, 537–555.

VEKSTEIN, G. E. 1998 Landau resonance mechanism for plasma and wind generated waves. *Am. J. Phys.* **66**, 886–892.